Development of a 3D Printed Gap Gauge with Embedded Force Sensor for Balancing Unicompartmental Knee Arthroplasty.

Dimitrios Kosmas[1], Hans-Peter van Jonbergen[2], Martijn Schouten[1], Momen Abayazid[1], Gijs Krijnen[1]
[1]Robotics And Mechatronics group, University of Twente, Enschede, The Netherlands
[2]Deventer Hospital, Orthopedics, Deventer, The Netherlands
Email: d.kosmas@utwente.nl

2021 IEEE Sensors | 978-1-7281-9501-8/21/$31.00 ©2021 IEEE | DOI: 10.1109/SENSORS47087.2021.9639727

***Abstract* - A novel gap-gauge with embedded sensing is developed for assisting in Oxford Unicompartmental Knee Arthroplasty (OUKA). A fully 3D printed differential capacitive sensor for normal forces is embedded into the Fused Deposition Modelling (FDM) fabricated body of the gap-gauge. The sensor consists of three conductive parallel-plates realizing two capacitive sensors with a common ground plate. It is demonstrated that for the set of specifications the 3D printed device is potentially suitable for the application. Minimal drift, weak non-linearity and hysteresis in the response are present. There is good agreement between the designed and true sensitivity.**

Keywords - 3D Printed Sensors, Fused Deposition Modelling, Oxford Unicompartmental Knee Arthroplasty, Capacitive Sensor, Normal, Force

I. Introduction

During a partial knee replacement surgery, the space between the femur and tibia is assessed with the help of a spoon shaped gap-gauge [1] (fig. 1). For that purpose, the gauges are classified in five size-defined categories, i.e X-small, small, medium, large and X-large. For each category several thicknesses exist ranging from $1\,\mathrm{mm}$ to $9\,\mathrm{mm}$ [2]. In order to achieve good clinical results it is crucial for the gap between the femoral and tibial component of the prosthesis to be equivalent at two key positions i.e., flexion and extension of the knee. For the longevity of the prosthesis it is also imperative that the normal force applied by the ligaments in both situations is similar as well as within a certain range. Currently the proper amount of applied force is assessed based on the friction felt by the orthopedist during the gauge insertion, or by the felt force applied when attempting to raise the gauge while inserted. Consequently, this phase of the procedure relies heavily on the experience of the orthopedist.

The state-of-the-art development of 3D printed sensors [3], [4] has proved the possibility of employing additive manufacturing to fabricate functional sensing and smart devices by means of multi-material FDM fabrication. Capacitive sensing has been shown to be less susceptible to drift, hysteresis and non-linearity [4]–[6]. In [7] single capacitive 3D printed force sensors reveal a relative linear response but drift is still present, possible due to material creep. Often, a differential readout has demonstrated to significantly reduce drift in the sensor response [8], [9]. In this work, the development of an embedded differential capacitive sensor based on FDM fabrication is presented. Depending on a set of specifications, the sensor is designed and fabricated. Finally, harmonic loading is used to characterize and assess the sensor's performance.

This work was made possible through funding from the Pioneers in Health Care (PIHC) fund and the collaboration between the Deventer Hospital and University of Twente.

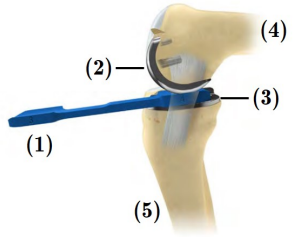

Fig. 1. Conventional gap-gauge usage during tibia to femur space assessment. Source: [1].(1) gap-gauge, (2) femoral prosthesis component, (3) tibial prosthesis component, (4) femur, (5) tibia.

II. Application

For the prototype the focus is on one of the most commonly used configurations in the surgery, which is medium sized with a thickness from $3\,\mathrm{mm}$ to $5\,\mathrm{mm}$.

In order to maintain the principal use of the gap-gauge, the least possible deformation is necessary. Conversely, a higher deformation potentially yields a higher sensor signal. For that reason, a maximum of $10\,\%$ deformation is specified by the orthopedist.

The appropriate normal force sensing range is obtained by means of an OUKA artificial setup. Once assessed by the orthopedist, the nominal applied force is found to be approximately $7.5\,\mathrm{N}$. Hence, the sensing force range of the prototype is set from $2\,\mathrm{N}$ to $12\,\mathrm{N}$.

III. Sensor

Towards low non-linearity and drift [4] a capacitive sensing principle in differential configuration is adopted. By assuming stiff electrode plates, compressible dielectrics and a small

978-1-7281-9501-8/21/$31.00 ©2021 IEEE

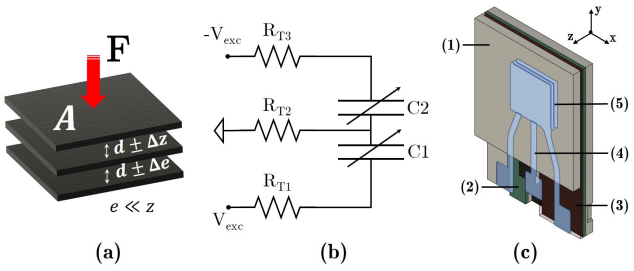

Fig. 2. (a) Parallel-plate differential configuration. Here, Δz and Δe describe the deformation as experienced from the top and bottom plates respectively. (b) Differential capacitive network with the in-series resistances $R_{\mathrm{T}1,3}$ introduced by the contact traces. (c) CAD design (Autodesk Fusion 360), (1) sensor body, (2,3) 1st and 2nd dielectric, (4) contact traces, (5) sensor plates.

displacement change $\Delta z \ll d$ [7], from the parallel-plate approximation the capacitance change is:

$$\Delta C = -\frac{\epsilon_0 \epsilon_{\mathrm{r}} A}{d^2}\Delta z = -\frac{\epsilon_0 \epsilon_{\mathrm{r}}}{dE'}F \tag{1}$$

where, ϵ_0 is the vacuum permitivity, ϵ_r the dielectric constant, A the electrode area, F the applied force and E' the effective Young's modulus. From eq. 1 the sensor sensitivity can be seen as the fraction $\epsilon_0 \epsilon_r A/dE'$ $\mathrm{F\,N^{-1}}$. The sensitivity is inversely proportional to the dielectric thickness d.

Considering the differential design, the total capacitance change can then be expressed as:

$$\begin{aligned}\Delta C_{\mathrm{total}} &= \Delta C_{\mathrm{b}} - \Delta C_{\mathrm{t}} \\ &= \left(\frac{\epsilon_{\mathrm{r_t}}}{E'_{\mathrm{t}}} - \frac{\epsilon_{\mathrm{r_b}}}{E'_{\mathrm{b}}}\right)\frac{\epsilon_0 A}{dA_{\mathrm{d}}}F\end{aligned} \tag{2}$$

with indices b and t denoting the bottom and top plates respectively, and A_{d} the area of the dielectrics (fig. 2c).

A. Design

The design of the concept sensor is shown in fig. 2c. The overall dimensions of the main body are 25 x 37 x $5\,\mathrm{mm}^3$. In this case, $5\,\mathrm{mm}$ thickness is selected in order to ease the fabrication and relax the tolerances for the initial design. The terminal and ground electrodes consist of three square parallel-plates with area $A = 100\,\mathrm{mm}^2$ and a thickness of $200\,\mu\mathrm{m}$. The dielectric thickness for both capacitors is set at $d = 600\,\mu\mathrm{m}$ and the surface area of the dielectric is $A_{\mathrm{d}} = 625\,\mathrm{mm}^2$. Given the Young's modulus of Ninjaflex TPU of $12\,\mathrm{MPa}$ [10] for $100\,\%$ infill, and the effective Young's modulus as calculated by [11] for $60\,\%$ infill, the estimated sensitivity for the target force range is then at $9.1\,\mathrm{fF\,N^{-1}}$.

To evaluate the effect of long contact traces, each of the electrode's contact points are displaced a distance of $\approx 25\,\mathrm{mm}$ from the plate center (fig. 2c). The added series resistances $R_{\mathrm{T}i}$ for the terminal electrodes is comprised of the equivalent series resistance (ESR) of each capacitor and the resistance of the contact trace. The ground electrode's series resistance is defined by the contact trace $R_{\mathrm{T}2}$ alone (fig. 2b).

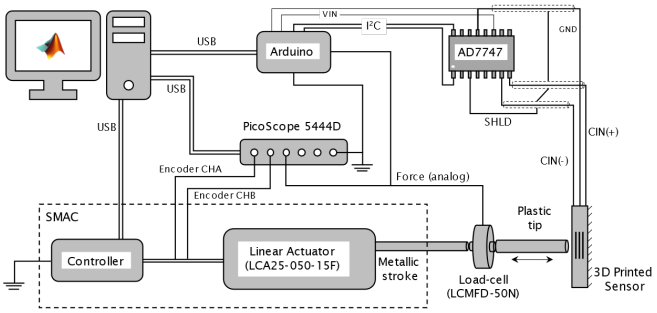

Fig. 3. Experimental setup overview

B. Fabrication

The sensor realization is based on a multi-material FDM method by means of the Diabase H-series 3D printer. A four material task is carried out, where generic PETG is used for the sensor body, NinjaFlex [10] and x60 [12] TPU for the dielectric of the bottom and top capacitors respectively and ProtoPasta conductive PLA [13] for all the electrodes. Global print settings are a *layer height* of $100\,\mu\mathrm{m}$ (only 1st layer of $300\,\mu\mathrm{m}$), *line width* of $0.4\,\mathrm{mm}$, build platform temperature of $75°$ C and *Z-hop* of $2\,\mathrm{mm}$. Table I describes the material specific high-level print settings as configured in Cura slicer equipped with a post-processor for the Diabase H-series [14]. Additionally, a prime tower is enabled as purge option during every tool and layer change. To enhance the limited performance of the default prime tower when used with > 2 materials, three blocks of $5\mathrm{x}10\,\mathrm{mm}$ are used as means to force priming at every layer and minimize filament mixing and contamination.

TABLE I. MATERIAL SPECIFIC RINTING PARAMETERS

	PETG	NinjaFlex	x60	ProtoPasta
Nozzle temperature [°C]	240	225	215	220
Infill density [%]	20	100	60	100
Flow [%]	100	120	125	100
Print speed [$\mathrm{mm\,s^{-1}}$]	45	25	20	30
Part cooling fan speed [%]	30	70	40	70
CAM dial position [-]	4	2	1	4

IV. EXPERIMENTAL SETUP

Fig. 3 shows an overview the experimental setup for characterization. The sensor (bottom right) is mechanically loaded along the z direction with a normal force applied by a linear actuator (SMAC LCA25-050, controlled by SMAC LCC-10 through MATLAB [15]). For accurate evaluation of the applied force, a load-cell (LCMFD-50N) is fixed at the stroke end. To provide guarding against interference from the actuator and the load-cell, a plastic tip with length of $4.8\,\mathrm{cm}$ is attached as the end-effector.

To readout the capacitance, the off-the-shelf AD7747 [16] capacitance-to-digital converter (CDC) is employed. The CDC provides differential measurement capabilities and a maximum capacitance per channel of up to $25\,\mathrm{pF}$. Given the sensor design, the estimated capacitance should be $\approx 7\,\mathrm{pF}$ allowing errors for unaccounted anisotropy and fringing effects. The CDC communicates with an Arduino Uno 8-bit microcontroller by means of the $\mathrm{I^2C}$ protocol [17] and is controlled by MATLAB through a serial interface.

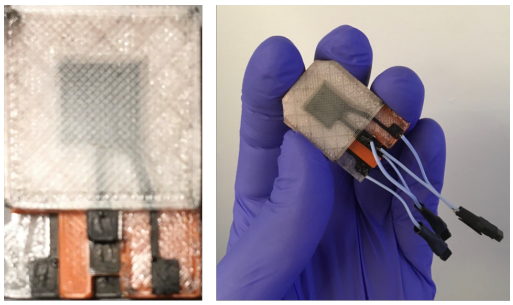

(a) (b)

Fig. 4. (a) Sensor as fabricated (not to scale), (b) post-processed sensor, ready for measurement and fixing in the experimental setup.

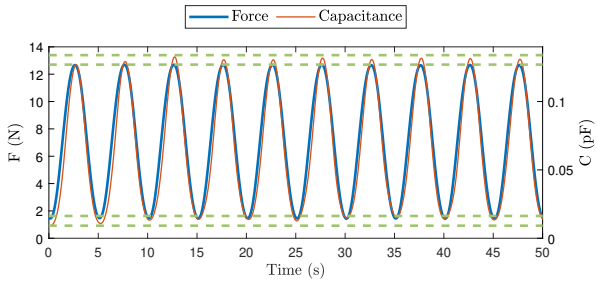

Fig. 5. Sinusoidal load excitation and capacitance response versus time. Green lines describe the variation range of the extrema throughout a run-time of 10 periods.

Additionally, a PicoScope 5444D digital oscilloscope is used to acquire the load-cell amplified (Futek IAA100) voltage output as well as the extracted raw encoder reading of the linear actuator, used to evaluate the stroke position.

V. Results

A. Fabricated sensor

The sensor requires minimal post-processing after fabrication, the main task being the attachment of short cables as means to connect the sensor to the CDC. There a several methods to attach cables to the 3D printed structure [4]. In this case, embedding wires by melting is chosen as it requires no additional assembly of parts and is mechanically relatively strong. The contact pads on the sensor are designed with a surface area of $3.8 \times 4.8\,\mathrm{mm}^2$ and braided wire is chosen in order to distribute the contact as evenly as possible across the pad. The bonded cables are then attached to SMB type shielded coaxial cables that lead to the AD7747 ports.

B. Experimental results

To characterize the sensor in terms of hysteresis, non-linearity and drift, a mechanical load in the form of a sinusoidal force with amplitude of $7\,\mathrm{N}$, offset of $5.5\,\mathrm{N}$ for force control, or an amplitude of $70\,\mu\mathrm{m}$ for position control is applied. For both cases the tested frequencies range from $0.1\,\mathrm{Hz}$ to $1\,\mathrm{Hz}$

MATLAB scripts are used to reconstruct the stroke position, filter the capacitance channel with a zero-phase 2^{nd} order low-pass Butterworth filter with cut-off frequency of $2.5\,\mathrm{Hz}$ and downsample the force signal to the sampling frequency of the CDC at $20\,\mathrm{Hz}$. The delay between the devices is determined by comparing the force signal as acquired from all devices in time-domain and used for signal synchronization.

1) Sinusoidal loading: Figure 5 shows the sensor response for a sinusoidal force during 10 periods of $T = 5\,\mathrm{s}$. The sensor follows the reference fairly well but shows slower response during loading phase in comparison to unloading, introducing hysteresis. Additionally, there are random variations towards the capacitance extrema, specifically, within an interval of $6.9\,\mathrm{fF}$ for the maxima and an interval of $7.1\,\mathrm{fF}$ for the minima.

From fig. 6 it is clear that both non-linearity and hysteresis are less compared to what may expected from piezoresistive approaches [8], [18]. The enclosed area of each normalized hysteresis loop is used as criterion to select two data sets. The first set represents the cycle with the closest to average area,

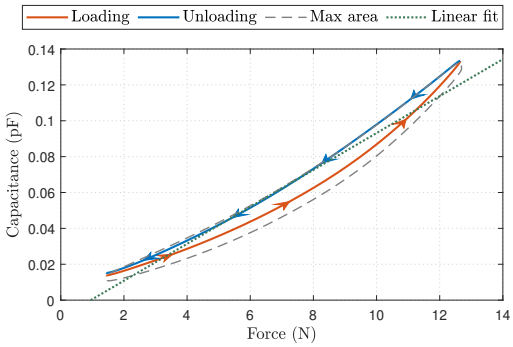

Fig. 6. Average (10^{th}) and max (1^{st}) loading cycle capacitance response at excitation frequency f =0.2 Hz

with value of $5.95\,\%$ ($100\,\%$ is defined by the unit square with origin at 0) and the second set represents the cycle where the area is largest, with a value of $10.93\,\%$.

Both figures 5 and 6 suggest that within the time-frame of the experiment ($50\,\mathrm{s}$) and given the differential read-out, short-term drift effects, often induced due to temperature variations within the material from the applied pressure, are of small magnitude and the capacitive response remains within the variation range as described in this section. Lastly, the fabricated sensor sensitivity is found to be $9.5\,\mathrm{fF\,N^{-1}}$ which is in close proximity to the designed sensitivity.

VI. Discussion and Conclusion

In this work, a 3D printed differential capacitive sensor for quantifying the normal compressive force applied to a gap-gauge when used during an OUKA surgery is presented. For the given set of specifications the sensor proves suitable for the application. There is good correspondence between the designed and fabricated sensor sensitivity. Only weak non-linearity is present in the response at low frequencies. Regarding hysteresis, even with the capacitive sensing the maximum error from a linear fit is $16.5\,\mathrm{fF}$ which results in significant loss in accuracy, therefore, for frequent repetitive measurements, methods of compensation are advised [4].

The proposed design allows the sensor to be embedded into the geometry of a conventional gap-gauge. Future work will look into compatible sterilization methods and sensor characterisation under static loads to evaluate the performance in practical application conditions.

REFERENCES

[1] J. Goodfellow, J. O'Connor, H. Pandit, C. Dodd, and D. Murray, *Unicompartmental arthroplasty with the Oxford knee*. Goodfellow Publishers LTD, 2011.

[2] Z. Biomet, "Oxford partial knee microplasty instrumentation." [Online]. Available: https://www.zimmerbiomet.com/content/dam/zimmer-biomet/medical-professionals/000-surgical-techniques/knee/oxford-partial-knee-microplasty-instrumentation-surgical-technique.pdf

[3] Y. Xu, X. Wu, X. Guo, B. Kong, M. Zhang, X. Qian, S. Mi, and W. Sun, "The Boom in 3D-Printed Sensor Technology," *Sensors (Basel, Switzerland)*, vol. 17, no. 5, pp. 1–37, 2017.

[4] M. Schouten, G. Wolterink, A. Dijkshoorn, D. Kosmas, S. Stramigioli, and G. Krijnen, "A review of extrusion-based 3d printing for the fabrication of electro- and biomechanical sensors," *IEEE Sensors Journal*, vol. 21, no. 11, pp. 12 900–12 912, 2021.

[5] X. Aeby, R. v. Dommelen, and D. Briand, "Fully FDM 3D Printed Flexible Capacitive and Resistive Transducers," *2019 20th International Conference on Solid-State Sensors, Actuators and Microsystems & Eurosensors XXXIII (TRANSDUCERS & EUROSENSORS XXXIII)*, no. June, pp. 2440–2443, 2019.

[6] R. van Dommelen, J. Berger, R. I. Haque, M. R. Binelli, G. de Freitas Siqueira, A. R. Studart, and D. Briand, "Fully 3d printed mechanical pressure sensors: A comparison of sensing mechanisms," *2020 IEEE SENSORS*, 2020.

[7] M. Schouten, R. Sanders, and G. Krijnen, "3D printed flexible capacitive force sensor with a simple micro-controller based readout," in *2017 IEEE SENSORS*, Oct 2017, pp. 1–3.

[8] D. Kosmas, M. Schouten, and G. Krijnen, "Hysteresis Compensation of 3D Printed Sensors by a Power Law Model with Reduced Parameters," in *FLEPS 2020 - IEEE International Conference on Flexible and Printable Sensors and Systems, Proceedings*, 2020.

[9] M. Schouten, P. Patel, R. Sanders, and G. Krijnen, *3D printed differential force and position sensor based on lossy transmission lines*. Transducers, 2021.

[10] F. Drives. (2021) Safety data sheet ninjaflex 3d printing filament. [Online]. Available: https://ninjatek.com/wp-content/uploads/NinjaFlex-TDS.pdf

[11] M. Schouten, C. Spaan, D. Kosmas, R. Sanders, and G. Krijnen, "3d printed capacitive shear and normal force sensorusing a highly flexible dielectric," in *Sensors Applications Symposium 2021*. IEEE, 2021-submitted.

[12] D. Engineering, 2021, https://www.diabasemachines.com/product-page/materials-60A and https://b8a4bbc5-5d2b-494d-b28a-de1f87376ff5.usrfiles.com/ugd/b8a4bb_50d3cc9169d64a71aabd12300fe30e2c.pdf.

[13] ProtoPlant, makers of Proto-pasta. Composite PLA - Electrically Conductive. https://www.proto-pasta.com/ and https://cdn.shopify.com/s/files/1/0717/9095/files/TDS__Conductive_PLA_1.0.1.pdf?1771.

[14] M. Schouten, "diabase_cura_post_processor," 2020. [Online]. Available: https://github.com/martijnschouten/diabase_cura_post_processor

[15] ——, "SMAC_LCA25-5-_MATLAB_driver," 2020. [Online]. Available: https://github.com/martijnschouten/lab-equipment-matlab-drivers/tree/master/SMAC\%20actuator

[16] 2021. [Online]. Available: https://www.analog.com/media/en/technical-documentation/data-sheets/AD7747.pdf

[17] P. Janko, "AD7747 I2C communication drivers ," 2020. [Online]. Available: https://github.com/jankop2/Arduino-AD7747

[18] J. Christ, N. Aliheidari, P. Pötschke, and A. Ameli, "Bidirectional and stretchable piezoresistive sensors enabled by multimaterial 3d printing of carbon nanotube/thermoplastic polyurethane nanocomposites," *Polymers*, vol. 11, no. 1, p. 11, 2018.